

Temperature dependence of hyperfine magnetic fields in Fe-Ni

B. Fultz* and J. W. Morris, Jr.

Materials and Molecular Research Division, Lawrence Berkeley Laboratory, and the Department of Materials Science and Mineral Engineering, University of California, Berkeley, California 94720

(Received 29 April 1985)

The ^{57}Fe hyperfine magnetic field (HMF) distribution in bcc Fe-Ni alloys was calculated with a model of linear response of the ^{57}Fe HMF to magnetic moments in the alloy. With the use of empirical parameters, the model largely accounts for the ^{57}Fe HMF distribution at low temperatures. As shown by experiments with Si solutes in Fe-Ni, the anomalously strong temperature dependence of the ^{57}Fe HMF in Fe-Ni is not due to the temperature dependence of the HMF response parameters. By analyzing the shape of the ^{57}Fe HMF distribution, we find that this anomalous temperature dependence results from a large thermal sensitivity of the magnetic moments at those Fe atoms with more Ni atoms as nearest neighbors. This correlated with a strong temperature dependence of the recoil-free fraction and the second-order Doppler shift in Fe-Ni. We suggest that the large mean-square thermal displacement of Fe atoms in Fe-Ni is the cause of the anomalously strong temperature dependence, and we offer two explanations for this effect. Additionally, we have found evidence for a pseudodipolar interaction in Fe-Ni, and we also discuss the problems of parametrizing the ^{57}Fe HMF solely in terms of the number of nearest neighbors of the ^{57}Fe atom.

I. INTRODUCTION

The temperature dependence of hyperfine magnetic field (HMF) distributions in Fe alloys formed the basis for previous Mössbauer and NMR spectrometric investigations.¹⁻⁹ For many solutes the temperature dependence of the HMF at ^{57}Fe nuclei near solute atoms is little different from that at ^{57}Fe nuclei away from solute atoms. However, for bcc Fe-Ni alloys the HMF at ^{57}Fe nuclei near Ni atoms is found to be anomalous in that it decreases more rapidly with temperature than for Fe atoms more distant from Ni atoms.^{1,2,5-7,9} Of these previous studies, the NMR measurements of Riedi^{6,7,9} are the most reliable. A well-resolved satellite in the NMR spectra was identified with ^{57}Fe nuclei having a third-nearest-neighbor (3NN) Ni atom, as was suggested earlier.¹⁰ The change of this perturbed ^{57}Fe HMF with respect to the HMF at Fe nuclei without Ni neighbors was accurately measured as a function of temperature. This NMR investigation was, however, confined to relatively low temperatures and low Ni concentrations. The previous Mössbauer spectrometric investigations of the temperature dependence of HMF's in Fe-Ni alloys are less reliable. Van der Woude and co-workers^{1,2} reported a low-temperature ^{57}Fe HMF in Fe-Ni alloys of smaller magnitude than in pure Fe, in contradiction with other studies,^{5-7,9-12} including the present one. Measurements by Vincze and Grüner⁵ are more consistent with the data of the present study. Unfortunately, their analysis of experimental data attributes distinct resonances to ^{57}Fe nuclei with specific numbers of 1NN and 2NN Ni solutes, but this is not physically realistic for Fe-Ni Mössbauer spectra at low temperatures.

Early investigations produced a general picture of how the ^{57}Fe HMF in alloys of Fe with 3d transition-metal solutes originates from a mechanism of core polarization and from a mechanism of conduction-electron polariza-

tion.^{13,14} In Sec. III, we describe a detailed model of how the ^{57}Fe HMF depends on the magnetic moments in an alloy.^{2,10,11,15-17} In Sec. IV A, we calculate the ^{57}Fe HMF distribution at low temperature, and compare it to the measured HMF distributions in bcc Fe-Ni alloys. Measurements of the HMF distribution at high temperatures are reported, and in Sec. IV C, we describe how the HMF distribution was simulated by assigning a temperature dependence to a parameter in the model. The systematics of this temperature dependence are important in applications of the Mössbauer effect for chemical analysis of Fe-Ni alloys. Further analysis of this temperature dependence can reveal temperature dependences of some electronic interactions important to the ferromagnetic properties of Fe-Ni.

II. EXPERIMENTAL PROCEDURES AND DATA PROCESSING

Specimen materials were prepared from 99.995% pure Fe and 99.95% pure Ni by melting measured amounts of these metals in new alumina crucibles under a back pressure of helium gas. To ensure chemical homogeneity of the ingots, the melt was held at 1923 K for 2 h, and cooled at 50°C/min to room temperature. Weight losses after melting were negligible, and discoloration was not observed on the ingot surfaces, so the alloy compositions were based on the weight of the starting materials. These compositions were checked with x-ray fluorescence spectrometry. Further homogenization of the ingots was performed by heating them in evacuated quartz ampules at 1423 K for 3 h, and then breaking the hot quartz ampules under water. The ingots were then cold rolled into foils of 40 μm thickness. These foils were austenitized in evacuated quartz ampules. A martensitic microstructure with a uniform 10 μm grain size was produced during the wa-

ter quench which terminated this second heat treatment. Finally the foils were chemically polished in 3 ml HF in 100 ml H₂O₂ of 30% concentration. With careful polishing technique, foils of 5–8 μm thickness were prepared. Thickness distortion was minimized by using thin specimens, and thickness distortion corrections were not performed on the experimental data. By using thin specimens, however, the parabolic intensity distortion characteristic of constant acceleration spectra was noticeable, but corrections for this effect were easily performed for all experimental spectra.

All Mössbauer spectra were obtained in transmission geometry with a constant-acceleration spectrometer. An ~100-mCi ⁵⁷Co in Rh and an ~100-mCi ⁵⁷Co in Pd radiation source were used during the course of this work. Thin specimens of pure Fe at 290 K had a full width at half maximum (FWHM) of 0.24 mm/sec for the $\pm\frac{3}{2} \rightarrow \pm\frac{1}{2}$ peaks (peak numbers 1 and 6). Mössbauer spectra at 4.2 and 77 K were obtained with the specimens in contact with liquid nitrogen or liquid helium in the tail section of a cryostat designed for γ-ray transmission. Vibrations of the long tubes in the cryostat broadened the spectral lines by about 0.04 mm/sec. Spectra at elevated temperatures were obtained with the specimen foils sandwiched between beryllium disks in the bore of an evacuated tube furnace. The temperature of the specimen in this furnace was not homogeneous at lower temperatures, and this caused severe line broadening. Consequently, our data at 473 K spectra are less reliable. However, peak numbers 1 and 6 of pure Fe spectra at 773 and 873 K had FWHM's of 0.25 mm/sec. Spectrum collection alternated between the Fe-Ni alloys and pure (99.995%) Fe foils. From the pure Fe spectra small long-term drifts of the Doppler velocity were identified and then used to determine corrections to the experimental spectra. The positions of the corrected peak numbers 1 and 6 are believed accurate to ±0.002 mm/sec. Our calculations of the HMF's in Fe-Ni alloys also used the pure Fe HMF as a reference, so these numerous pure Fe spectra improved the connection between the calculations and the measurements.

The total absorption in the spectrum was measured in order to study the temperature dependence of the recoil-free fraction (RFF). By obtaining spectra with the same specimen and experimental configuration at two different temperatures, the ratio of recoil-free fractions at the two temperatures was found. Variations in detector performance led to scatter in the total absorption measurements of ±4% STD. We have only performed enough experiments to gain confidence in the RFF ratios of pure Fe and an Fe–9 at.% Ni alloy, but the other Fe-Ni alloys showed the same trend.

Determining the shape of the HMF distribution requires corrections of the experimental spectra for broadening of the absorption peaks due to the linewidth of the incident γ rays and the natural linewidth of the ⁵⁷Fe in the specimen. These corrections were performed in two ways. In the first method a Lorentzian function of width determined from a pure Fe spectrum was deconvolved from the spectrum by using the deconvolution theorem of harmonic analysis. Because high-frequency components

in the Fourier transform are emphasized in the deconvolution procedure, it was necessary to attenuate the deconvolution at high frequencies in order to prevent statistical scatter from dominating the deconvolution.¹⁸ The second method of extracting moments of HMF distributions from experimental spectra involved direct fittings of Lorentzian functions to the experimental data. Parameters of the simulated Mössbauer peaks were varied to minimize the root-mean-squared deviation between the simulated and experimental peaks. Data scatter was observed to affect the outcome of the curve-fitting procedure by occasionally causing the fitting program to get trapped in a local minimum of the root-mean-squared deviation.¹⁸

The first and sixth peaks in our Mössbauer spectra are not identical in shape because of local isomer shifts, so properties of the first and sixth peaks were averaged in order to obtain properties of the Fe-Ni HMF distribution. Although the local isomer shift and the HMF of a particular ⁵⁷Fe nucleus both depend on arrangements of neighboring solute atoms, we have had mixed quantitative success in associating a particular isomer shift with a particular HMF. However, qualitative trends can be deduced by inspection of the first and sixth peaks of the spectrum. For example, at low temperatures the width of the first peak in the Fe-Ni spectrum is greater than the width of the sixth peak. This means that the isomer shift of those ⁵⁷Fe nuclei having the larger HMF's is more negative than the isomer shift of those ⁵⁷Fe nuclei having the smaller HMF's.

III. ⁵⁷Fe HMF in bcc Fe ALLOYS

The important contributions to the ⁵⁷Fe HMF in Fe-based alloys arise from the Fermi contact interaction: the spins of electrons that interpenetrate the ⁵⁷Fe nucleus interact with the nuclear spin to perturb the nuclear energy levels. Contributions to the ⁵⁷Fe HMF come from spin polarizations of the 1s, 2s, 2p, 3s, and 4s electrons, whose wave functions are nonvanishing at the nucleus. A neighboring Ni atom changes the magnetic moment at the ⁵⁷Fe atom by changing its balance of 3d↑ and 3d↓ electrons. Through intra-atomic exchange interactions, an increased fraction of 3d↑ electrons will reduce the Coulomb repulsion between the 3d↑ electrons and 1s↑, 2s↑, 2p↑, 3s↑ core electrons, and the 4s↑ conduction electrons, changing their radial distribution about the ⁵⁷Fe nucleus. Different systematics of exchange interactions affect the spin-down electrons. A change in the spin polarization of those electrons which interpenetrate the ⁵⁷Fe nucleus is developed in proportion to the change in magnetic moment at the ⁵⁷Fe atom. From theoretical^{19,20} and experimental studies, the net effect on the ⁵⁷Fe HMF due to a solute-induced change in the number of unpaired 3d electrons local to the ⁵⁷Fe atom, ΔH_L, is found to be

$$\Delta H_L = (\alpha_{CP} + \alpha_{CEP})\Delta\mu(0), \quad (1)$$

$$\Delta H_L \approx -(90 \text{ kG}/\mu_B)\Delta\mu(0). \quad (2)$$

The change in magnetic moment at the ⁵⁷Fe atom, located at the origin of our bcc lattice, is Δμ(0). The constants α_{CP} and α_{CEP} relate changes in the ⁵⁷Fe HMF to changes

in $\Delta\mu(0)$ through the mechanisms of core polarization and conduction-electron polarization, respectively. We reference ΔH_L to the local contribution to the ^{57}Fe HMF in pure Fe metal.

The spin polarization at the ^{57}Fe nucleus due to the nonlocalized $4s$ electrons is also sensitive to magnetic moments at neighboring atoms. For solutes with atomic volumes similar to that of Fe, these changes in $4s$ contributions to the ^{57}Fe HMF upon alloying are proportional to the difference between the magnetic moment of the neighboring atom $\mu(r)$, and the magnetic moment of an Fe atom in pure Fe, μ_{Fe} . With respect to pure Fe, the change in the ^{57}Fe HMF due to neighboring (nonlocal) magnetic moments in the alloy, ΔH_{NL} , is

$$\Delta H_{\text{NL}} = \alpha_{\text{CEP}} \sum_{r(\neq 0)} f(r) [\mu(r) - \mu_{\text{Fe}}(r)], \quad (3)$$

where $f(r)$ is the fraction of conduction-electron polarization at the ^{57}Fe nucleus produced by a change in magnetic moment at r , with respect to the conduction electron polarization produced by the same change in magnetic moment at $r=0$.

For further analysis it is convenient to express ΔH_{NL} as the sum of two terms. The first term comprises the contributions from those neighboring lattice sites occupied by solute atoms, ΔH_{DNL} (direct nonlocal), and the second term comprises the contribution from those neighboring lattice sites occupied by Fe atoms, ΔH_{INL} (indirect nonlocal):

$$\Delta H_{\text{NL}} = \Delta H_{\text{DNL}} + \Delta H_{\text{INL}}$$

$$\Delta H_{\text{DNL}} = \alpha_{\text{CEP}} \sum_{r(\neq 0)} \left[f(r) \delta(r) \times \left[\mu_X + \sum_{r'} \delta(r') g_X^X(r' - r) - \mu_{\text{Fe}} \right] \right], \quad (4a)$$

$$\Delta H_{\text{INL}} = \alpha_{\text{CEP}} \sum_{r(\neq 0)} \left[f(r) [1 - \delta(r)] \sum_{r'} \delta(r') g_X^{\text{Fe}}(r' - r) \right]. \quad (4b)$$

The Kronecker δ function equals 1 if the site is occupied by a solute atom, and equals 0 if it is occupied by an Fe atom. We use the variable $g_X^Y(r)$ to represent the change in magnetic moment of a Y atom when it has an X solute atom in its r th coordination sphere. The additivity of the $g_{\text{Ni}}^{\text{Fe}}(r)$ parameters is expected only for dilute Fe-Ni alloys; we will later discuss saturation of the Fe magnetic moments. All perturbations of Fe magnetic moments are referenced to the magnetic moment of an Fe atom in pure Fe, μ_{Fe} , and all perturbations of the X magnetic moments are referenced to the magnetic moment of an isolated X atom in an Fe matrix, μ_X .

In accordance with previous investigations, the same $\{\alpha_{\text{CEP}} f(r)\}$ parameters are used in both Eqs. (4a) and (4b). This implicitly assumes one unpaired spin at an Fe atom or one unpaired spin at a solute atom to be equally effective

in polarizing the $4s$ electrons. This assumption is adequate for solute atoms which develop no local magnetic moment in bcc Fe (i.e., Si, Ge, Al) because they do not polarize the $4s$ electrons, and the specific parameters $\{\alpha_{\text{CEP}} f(r)\}$ associated with them is immaterial. However, as discussed below, our data suggest that in Fe-Ni alloys, the Ni atoms are inherently less effective in polarizing the $4s$ electrons than are Fe atoms.

In a nondilute disordered alloy there will be many solute atom environments contributing to a distribution of ^{57}Fe HMF's. It is often adequate to parameterize the HMF at a ^{57}Fe nucleus in terms of the numbers of solute atoms in its various nearest-neighbor shells, $\{n(r)\}$. When the solutes are randomly distributed with an average concentration c , there will be a probability, $P(\{n_j\}, c)$, of a specific set of nearest-neighbor shell occupancies $\{n'_1, n'_2, n'_3, \dots\}$ equal to the product of the binomial probabilities associated with the occupancy of each nearest-neighbor shell:²²

$$P(\{n_j\}, c) = \prod_{j(\neq 0)} \frac{N_j!}{(N_j - n_j)! n_j!} c^{n_j} (1 - c)^{N_j - n_j}. \quad (5)$$

For the bcc structure the total number of sites in consecutive nearest-neighbor shells form an ordered set $\{N_j\}$, which begins $\{8, 6, 12, 24, 8, 6\}$.

The ^{57}Fe HMF is determined by the locations of the solute atoms [Eq. (5)] and the systematics of how they perturb the ^{57}Fe HMF [Eqs. (1)–(4)]. With this prescription we can evaluate the constants $\{\alpha_{\text{CEP}} f(r)\}$. For such "calibration" purposes it is convenient to study alloys of Fe-Si. Si atoms (and other sp -series solutes such as Al and Ge) develop no magnetic moment in bcc Fe, so the parameters $g_{\text{Si}}^{\text{Si}}(r)$ and $(\mu_{\text{Si}} - \mu_{\text{Fe}})$, which determine H_{DNL} , are known to be 0 and $2.22\mu_B$, respectively. Furthermore, since $\{g_{\text{Si}}^{\text{Fe}}(r)\} \approx 0$,^{23–25} ΔH_L and ΔH_{INL} can conveniently be neglected. Without $\{g_X^{\text{Fe}}(r)\}$ parameters that broaden the HMF effects from each set $\{n_j\}$, the Mössbauer spectra from dilute Fe-Si alloys show well-defined satellite peaks that can be associated with a Si atom in each nearest-neighbor shell. Measuring the positions of these satellite peaks determines the set $\{\alpha_{\text{CEP}} f(r)\}$.

^{57}Fe HMF's in alloys with solutes that perturb neighboring Fe magnetic moments (i.e., $\{g_X^{\text{Fe}}(r)\} \neq 0$) can also be parametrized with the set $\{n_j\}$, provided that the solute concentrations are low enough to obviate questions of how a solute atom affects the magnetic moment disturbance around another solute atom. Even so, in the case of Ni the $\{g_{\text{Ni}}^{\text{Fe}}(r)\}$ parameters are large, and it is necessary to accurately account for ΔH_{INL} . This was done in detail by Stearns with NMR spectra of dilute Fe-Ni alloys obtained by Budnick *et al.* at 1.4 K.^{10,16} The total HMF perturbation due to a solute in specific nearest-neighbor shells was calculated for various values of constrained μ_{Ni} and $\{g_{\text{Ni}}^{\text{Fe}}(r)\}$ parameters. A good fit of the calculated spectra to the experimental spectra was found for rather precise values of μ_{Ni} and $\{g_{\text{Ni}}^{\text{Fe}}(r)\}$. These values of μ_{Ni} and $\{g_{\text{Ni}}^{\text{Fe}}(r)\}$ were about 30% larger than experimental values obtained from neutron diffuse magnetic scattering. Stearns and Feldkamp²⁶ later showed that the lower value

of μ_{Ni} from the neutron studies is a consequence of wavelength limitations in the neutron scattering experiments. We believe that the lower values of $\{g_{\text{Ni}}^{\text{Fe}}(r)\}$ measured by the neutron scattering experiments are a consequence of obtaining these data at room temperature.

The distinct HMF structure observed in high resolution NMR spectra of dilute Fe-Ni alloys is not evident in Mössbauer spectra of nondilute Fe-Ni alloys, and the HMF distribution is best parameterized in terms of its mean, variance, and skewness. Vincze, Campbell, and Meyer¹² measured the mean of the Fe-Ni HMF distribution, and used average values of magnetic moments to determine an average HMF. The problem of calculating the full HMF distribution, rather than just the mean HMF, is more complicated because the ΔH_{INL} contribution from a specific solute environment cannot be simply parameterized by the set $\{n_j\}$. The difficulty is that the magnetic moment disturbance around a Ni solute encompasses many atoms, so even at low solute concentrations the magnetic effects from different Ni atoms will interfere. Because a Ni solute atom causes no magnetic moment disturbance at another Ni solute atom, but would have caused a magnetic moment disturbance at an Fe atom replaced by the other Ni atom, the magnetic moment disturbance around a Ni atom will vary with the positions of the other Ni atoms around it. Only if the solute atom causes the same magnetic moment perturbation at Fe atoms as at other solute atoms [i.e., unless $\{g_X^{\text{Fe}}(r)\} = \{g_X^{\text{Ni}}(r)\}$ as for Si solutes], the magnetic moment disturbance around a solute atom in a nondilute alloy cannot be deduced from the set $\{n_j\}$, except in an average way. Because $\{g_{\text{Ni}}^{\text{Fe}}(r)\} \gg \{g_{\text{Ni}}^{\text{Ni}}(r)\}$, the HMF's of nondilute Fe-Ni alloys are particularly unsuitable for parameterization by the set $\{n_j\}$. Detailed consideration of the locations of Ni atoms in the bcc structure is required in order to properly evaluate ΔH_{INL} . This is most conveniently accomplished by simulation with a digital computer.

Our computer simulation of the ^{57}Fe HMF included all atoms up to the 14NN shell around the ^{57}Fe atom. It was unfeasible to consider all possible arrangements of solute atoms over these sites, so a Monte-Carlo-type simulation was used. All sites around the ^{57}Fe atom were filled at random with solute atoms with a probability equal to the solute concentration. The magnetic moments of the atoms in the first three nearest-neighbor shells of the ^{57}Fe atom were calculated by accounting for solute-induced magnetic moment perturbations through their fifth nearest-neighbor shell. Knowing the type of atom and the magnetic moment at each site in the first three nearest-neighbor shells around the ^{57}Fe atom enabled calculation of the ΔH_{DNL} and the ΔH_{INL} contributions to the ^{57}Fe HMF. The ΔH_L contribution was evaluated by considering the effects of all solute atoms throughout the first five nearest-neighbor shells on the magnetic moment at the ^{57}Fe atom. Finally, the net hmf perturbation from this arrangement of solute atoms was recorded, and a new random arrangement of solute atoms was generated. This process continued for several thousand solute atom arrangements until a well-defined distribution of ^{57}Fe HMF perturbations was obtained.

IV. RESULTS AND DISCUSSION

A. Low-temperature ^{57}Fe HMF distribution

A binary Fe-1.5 at. % Si alloy was prepared for our measurements of the set $\{\alpha_{\text{CEPF}}(r)\}$ for pure Fe from 4 to 874 K. Distinct satellite peaks due to ^{57}Fe nuclei with neighboring Si atoms are seen on the lower Doppler shift energy sides of the absorption peaks in Fig. 1. These satellite peaks can be isolated from the main absorption peaks with a difference spectrum technique. A pure Fe spectrum was normalized and its velocity axis was slightly expanded so that the pure Fe peaks fit the high Doppler shift energy side of the Fe-1.5 at. % Si spectrum. The difference of these two spectra is also shown in Fig. 1. The difference intensity around the first absorption peak appears as two satellite peaks. The intensities of the two satellites are consistent with the probability of finding one Si atom in the 1NN shell and one Si atom in the 2NN shell. By approximately resolving the difference spectrum intensity around the sixth peak into 1NN and 2NN satellites, we obtain $\alpha_{\text{CEPF}}(r_1) = -11.5 \text{ kG}/\mu_B$ and $\alpha_{\text{CEPF}}(r_2) = -3.5 \text{ kG}/\mu_B$, in reasonable agreement with previously reported data.^{5,11,15} Solute sites at more distant nearest-neighbor sites do not produce distinct structure in the Mössbauer spectrum, and we account for them by the velocity scale expansion before differencing. This is frequently expressed as a concentration-dependent shift of the main absorption peak, dH_0/dc .^{10,11} For use in our computer simulation, but perhaps somewhat arbitrarily, we attribute dH_0/dc entirely to 3NN Si solutes through the relationship

$$\frac{dH_0}{dc} = \alpha_{\text{CEPF}}(r_3)12(-2.2\mu_B). \quad (6)$$

Our value for dH_0/dc of $+60 \text{ kG}/\mu_B$ is about half that reported in Ref. 11, but our $\alpha_{\text{CEPF}}(r_3)$ of $+2.5 \text{ kG}/\mu_B$ is in good agreement with that reported in Ref. 15. We found variations of 1–2 kG/μ_B in the $\alpha_{\text{CEPF}}\{f(r_j)\}$ parameters when the same difference procedure was applied to our Fe and Fe-Si spectra of lower statistical quality taken at 4, 77, and 873 K.

We investigated whether the $\alpha_{\text{CEPF}}(r_j)$ parameters de-

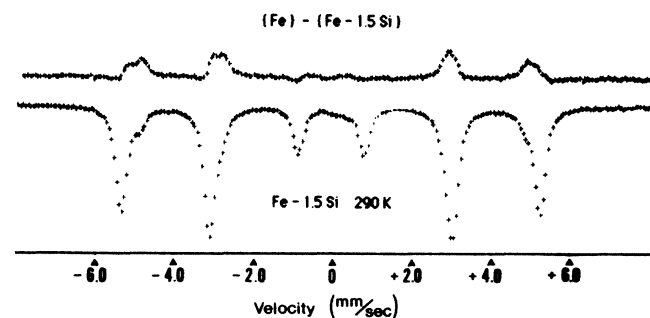


FIG. 1. Bottom: spectrum of Fe-1.5 at. % Si at 290 K. Top: difference of spectrum of pure Fe and spectrum of Fe-1.5 at. % Si. (Same scales of abscissa and ordinate for top and bottom.)

duced from dilute Fe-Si alloys are still appropriate for Fe-Ni alloys. Alloys of composition Fe-6.02 at. % Ni-1.5 at. % Si and Fe-8.86 at. % Ni-1.4 at. % Si were prepared, and their Mössbauer spectra were subtracted from spectra of Fe-6.02 at. % Ni and Fe-8.86 at. % Ni alloys taken at the same temperature to reveal Si satellite intensities in the Fe-Ni-Si alloys. The $\alpha_{\text{CEPF}}(r_j)$ parameters of Fe-Si, $\{-11.5, -3.5, +2.5, 0, \dots\}$ kG/ μ_B , adequately accounted for the observed difference intensity at 4, 77, and 290 K. Essentially the same results were obtained from Mössbauer spectra of Fe-Ni-Si specimens at 773 K; the parameters $\alpha_{\text{CEPF}}(r_1)$ and $\alpha_{\text{CEPF}}(r_2)$ were about -2 kG/ μ_B larger than those obtained at lower temperatures, but this may be comparable to the experimental error. An example of a Mössbauer spectrum from Fe-6.02 at. % Ni-1.5 at. % Si taken at 773 K is shown in Fig. 2, together with the difference between this spectrum and a Fe-6.02 at. % Ni spectrum. The similarity of the difference spectra in Figs. 1 and 2 is clear, so the $\{\alpha_{\text{CEPF}}(r_j)\}$ parameters must be similar.

Using the parameters reported by Stearns,^{15-17,27} the mean shift of the HMF distribution in all Fe-Ni alloys with respect to pure Fe was calculated to be about 15% larger than that measured at cryogenic temperatures. A similar discrepancy was reported by Stearns.²⁸ The width of the calculated HMF distribution was about 30% narrower than observed, but the calculated near-zero skewness was in agreement with observation. The use of our own $\{\alpha_{\text{CEPF}}(r)\}$ parameters gave the same results. Some workers^{3,17,29} have favored an alternate set of $\alpha_{\text{CEPF}}(r_j)$ parameters with a weak 2NN parameter and a negative 3NN parameter such as $\{\alpha_{\text{CEPF}}(r_j)\} = \{-11.0, -0.9, -2.4, +2.0, +1.1\}$ kG. The first three of these parameters were used in our calculations with reasonable success; the mean ^{57}Fe HMF in Fe-Ni was about 10% larger than with our set: $\{-11.5, -3.5, +2.5\}$ kG. The addition of the positive 4NN and 5NN parameters would produce better agreement, however.

We note that since δH_L [Eq. (1)] involves electrons local to the ^{57}Fe atom, it is not expected to change with Ni concentration. Some disagreement in the literature exists over the value of the combined HMF response parameter of Eq. (1) for dilute Fe-*X* alloys, and a value of ~ 70 kG/ μ_B was found to bring the calculated mean of the

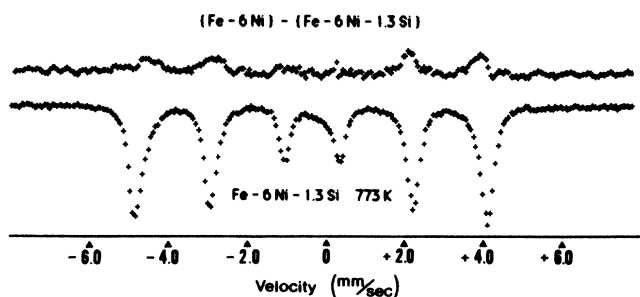


FIG. 2. Bottom: spectrum of Fe-6.02 at. % Ni-1.3 at. % Si at 290 K. Top: difference of spectrum of Fe-6.02 at. % Ni and spectrum of Fe-6.02 at. % Ni-1.3 at. % Si. (Same scales of abscissa and ordinate for top and bottom.)

^{57}Fe HMF distribution into better agreement with our experimental data. The calculated width becomes even narrower, however.

Variations of the magnetic moments and the magnetic moment perturbations which are consistent with magnetization and neutron diffraction data allow for small changes in the HMF distribution. In particular, variations of the individual parameters $g_{\text{Ni}}^{\text{Fe}}(r_j)$ did not have a significant effect on the HMF distribution, provided the total perturbation of Fe magnetic moments around a Ni atom, $\sum_j N_j g_{\text{Ni}}^{\text{Fe}}(r_j)$, was kept constant at $1.8\mu_B$. This condition was met by a second set of magnetic moment perturbations

$$\{g_{\text{Ni}}^{\text{Fe}}(r_j)\} = \{0.070, 0.056, 0.025, 0.018, 0.015, 0, \dots\},$$

which was more characteristic of the shape of the magnetic defects found from neutron scattering experiments.^{25,30,31} Simulations which used this second set gave HMF distributions essentially identical to those obtained with Stearns's parameters. Because the HMF distribution depends mainly on the sum of the $g_{\text{Ni}}^{\text{Fe}}(r_j)$ parameters rather than on their individual values, analysis of the HMF distribution obtained from Mössbauer spectra is not a particularly sensitive method for determining the shape of the magnetic moment disturbance around Ni solutes.

The small discrepancy between the measured HMF distribution and the calculated HMF distribution with Stearns's parameters could be explained by the uncertainties in the parameters in the model. However, much better simulations of the HMF distribution at low temperatures were obtained when we assumed that a magnetic moment at a Ni atom is only 70% as effective in polarizing the conduction electrons at the ^{57}Fe nucleus than the same magnetic moment at an Fe atom. This assumption is not unreasonable because the more compact 3*d* wave functions of Ni atoms are expected to produce a more localized spin polarization of the conduction electrons. Figure 3 compares first and sixth peaks of an experimental spectrum with peaks which were stimulated by using these smaller $\alpha_{\text{CEPF}}(r_j)$ parameters for Ni atoms, but us-

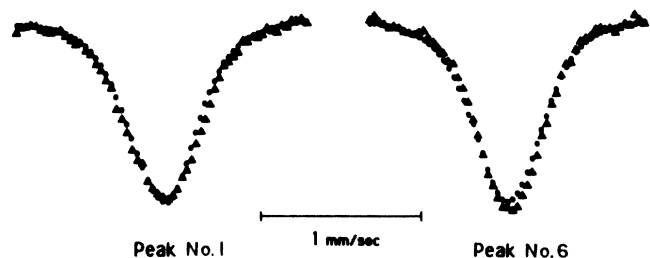


FIG. 3. Comparison between experimental and simulated peaks of Fe-8.86 at. % Ni. Simulation used the parameters $\mu_{\text{Fe}} = 2.22\mu_B$, $\mu_{\text{Ni}} = 1.4\mu_B$, $(\alpha_{\text{CP}} + \alpha_{\text{CEP}}) = -90$ kG/ μ_B . Fe: $\{\alpha_{\text{CEPF}}(r)\} = \{-11.5, -3.5, +2.5\}$ kG/ μ_B ; Ni: $\{\alpha_{\text{CEPF}}(r)\} = \{-8.5, -2.5, +1.8\}$ kG/ μ_B ; $\{g_{\text{Ni}}^{\text{Fe}}\} = \{0.070, 0.056, 0.025, 0.18, 0.15\}\mu_B$; $\{g_{\text{Ni}}^{\text{Ni}}\} = \{0\}$. Saturation of Fe magnetic moments was chosen to provide a bulk saturation magnetization of $2.9\mu_B$ for Fe-9 at. % Ni.

ing all the other parameters of Stearns. This assumption was somewhat more important when the alternate set $\{\alpha_{\text{CEP}}f(r_j)\} = \{-11.0, -0.9, -2.4\}$ was used.

The magnetic moments at Fe atoms do not increase linearly with increasing numbers of Ni neighbors. A linear increase predicts that the bulk saturation magnetization, μ_{sat} , increases with Ni concentration as

$$\mu_{\text{sat}} = c\mu_{\text{Ni}} + (1-c)\mu_{\text{Fe}} + c(1-c) \sum_{r_j(\neq 0)} N_j g_{\text{Ni}}^{\text{Fe}}(r_j). \quad (7)$$

Since the $\{g(r)\}$ parameters and Ni magnetic moments were chosen so that μ_{sat} agrees with magnetization data,¹⁶ their substitution into Eq. (7) provides an accurate description of how μ_{sat} depends on c_{Ni} when c_{Ni} is small. For Ni concentrations greater than 5 or 6%, however, μ_{sat} from Eq. (7) lies progressively higher than the experimental data.³²⁻³⁴ Because the Ni magnetic moment is independent of c_{Ni} ,³⁵⁻³⁷ the $g_{\text{Ni}}^{\text{Fe}}(r)$ parameters must be reduced with increasing c_{Ni} . The mean HMF is calculated to be more sensitive to this saturation of Fe moments than is the bulk saturation magnetization and this is seen in the reduced slope in Fig. 4 after 5–6% Ni. Several forms of saturation behavior were included in our simulation of the ⁵⁷Fe HMF, from a simple cutoff of Fe magnetic moment enhancements at some critical value, to more gradual roll-offs of the $\{g_{\text{Ni}}^{\text{Fe}}(r)\}$ parameters with increasing number of Ni neighbors. All saturation behaviors were capable of simultaneously providing good results for both the saturation magnetization and the HMF distribution over the composition range of 6–12% Ni.

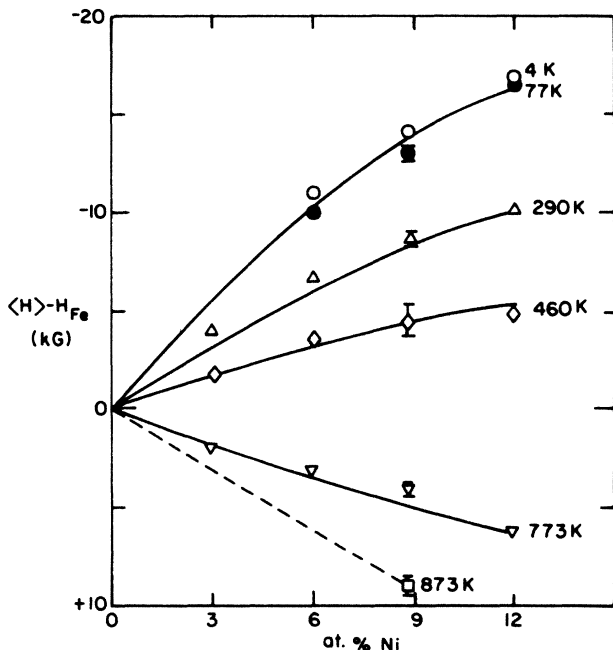


FIG. 4. Mean difference between HMF of Fe-Ni and pure Fe. Solid lines are the mean of the simulated HMF as calculated with the parameters of Fig. 3 and a reduction of the $\{g_{\text{Ni}}^{\text{Fe}}(r)\}$ parameters by the factors 1.0, 0.7, 0.1, and -0.2 at 4, 290, 773, and 873 K, respectively.

B. Temperature dependence of the recoil-free fraction, the second order Doppler shift, and the isomer shift

Our measurements of the net absorption in Mössbauer spectra were used to obtain the relative temperature dependences of the recoil-free fraction (RFF) in pure Fe and in Fe-9 at. % Ni. With a relative RFF of 1.0 at 4 K, relative RFF's of 0.89 at 290 K and 0.68 and 773 K were found for pure Fe metal, in good agreement with the original data of Preston *et al.*³⁸ The relative RFF's of Fe-9 at. % Ni were 1.0, 0.81, and 0.57 at 4, 290, and 773 K, respectively. The stronger temperature dependence of the RFF in Fe-9 at. % Ni than in pure Fe is statistically significant. The RFF depends on the mean squared thermal displacement, $\langle x^2 \rangle$, as $e^{-k_{\gamma}^2 \langle x^2 \rangle / 3}$. Using the Debye model to calculate $\langle x^2 \rangle$, the stronger temperature dependence of the RFF of the Fe-9 at. % Ni alloy indicates that its effective Debye temperature is about 70 K lower than that of pure Fe. This reduction in RFF may be due to localized phonons. The change in bulk modulus with Ni concentration³⁹ accounts for a reduction in Debye temperature of only 20 K for an Fe-9 at. % Ni alloy.

Differences between the mean of the entire Fe-Ni Mössbauer spectrum and the mean of the entire pure Fe spectrum are shown in Fig. 5. The shifts of Fe-Ni spectra with respect to pure Fe spectra are seen to be strongly temperature dependent. Assuming that the lattice forces are harmonic, the second-order Doppler shift (SODS) is proportional to the heat energy per unit mass of the material. We estimated the total heat energy at temperatures of interest with the Debye model. The 70 K reduction in Debye temperature of the Fe-9 at. % Ni alloy with respect to pure Fe, obtained from our RFF data, implies that the SODS difference between Fe-9 at. % Ni and pure Fe will be 0.011 mm/sec at 290 K and 0.018 mm/sec at 773 K. These SODS differences account for most of

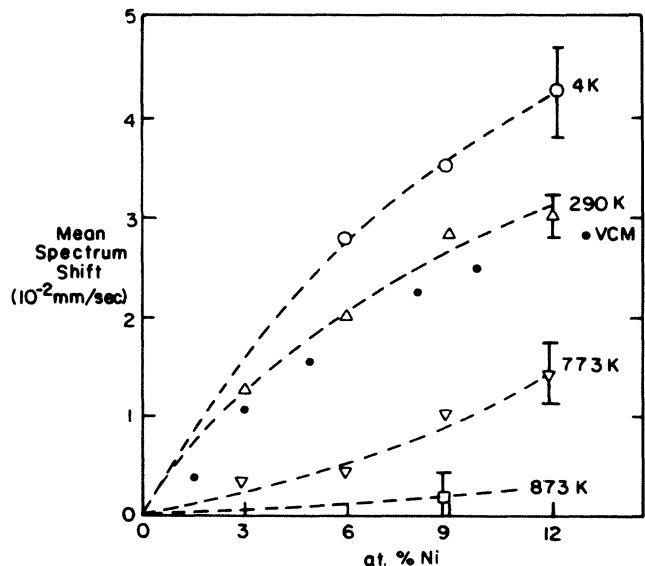


FIG. 5. Mean shift of the entire spectrum of Fe-Ni with respect to the entire pure Fe spectrum. The data labeled "VCM" are from Ref. 12.

the temperature dependence of the average spectrum shift of Fe-9 at. % Ni (Fig. 5). However, it appears that some of the temperature dependence of the mean spectrum shift could be due to a temperature dependence of the isomer shift at those ^{57}Fe nuclei with Ni neighbors. In charge transfers between Fe and Ni, the net increase in $3d$ electron density and the proportional loss of $4s$ electron density at the ^{57}Fe nucleus⁴⁰ will produce a positive isomer shift. After accounting for the effect of the SODS, the data of Fig. 5 suggest a reduction in this positive isomer shift as these charge transfers are reduced with temperature.

C. Temperature dependence of the ^{57}Fe HMF distribution

The first and sixth peaks of Mössbauer spectra of Fe-9 at. % Ni and pure Fe at different temperatures are shown in Fig. 6. The first peak of the Fe-Ni spectrum and the first peak of the pure Fe spectrum were normalized to have the same dip, and the sixth peaks are shown with this same normalization. At 4 K the Fe-Ni peaks are broadened and shifted towards larger velocities with

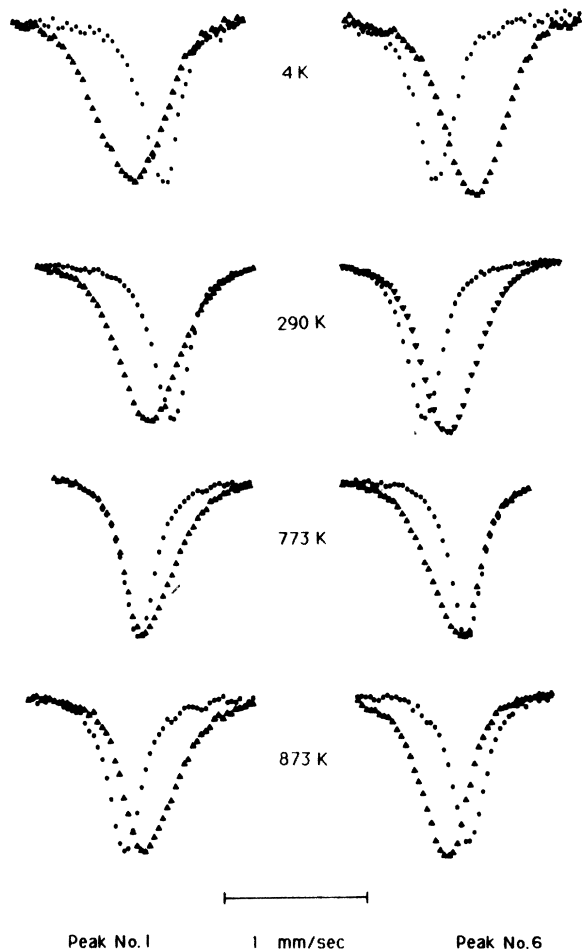


FIG. 6. Peak numbers 1 and 6 of Fe-Ni spectra positioned with respect to peak numbers 1 and 6 of pure Fe at the temperatures 4, 290, 773, and 873 K.

respect to the pure Fe peaks. Noticeable reductions in this broadening and shift are observed at 290 K. A qualitative change is seen in Fe-Ni peaks at 773 K, which are shifted toward smaller velocities with respect to pure Fe, and have become observably narrower. Additionally, at 773 K the first and sixth peaks of the Fe-Ni Mössbauer spectrum have very nearly the same dip, and are nearly mirror symmetric about the center of the spectrum. At higher temperatures the Fe-Ni peaks are further shifted toward smaller velocities, but have begun to broaden again.

Figure 4 shows the difference between the mean hmf of Fe-Ni alloys and that of pure Fe metal. The Lorentzian curve fitting procedure and the deconvolution procedure provided essentially the same results, which are averaged in Fig. 4. Figure 7 shows the width of the ^{57}Fe HMF distribution in Fe-Ni alloys obtained by taking the difference of the averaged FWHM of the first and sixth peaks of Fe-Ni and the FWHM of the first and sixth peaks of pure Fe. The variance of the HMF distribution obtained from the Lorentzian curve fitting procedure and the deconvolution procedure showed the same trends as in Fig. 7. Unfortunately, the variance and skewness were rather sensitive to the limits of numerical integration, so their numerical values are considered to be less useful to other investigators. The skewness of the HMF distribution at 4 and 290 K was small, and seems to change sign from negative to positive when the Ni concentration becomes greater than about 6%. However, the skewness at 773 and 873 K was larger, and was positive for all Ni concentrations.

Following the successful simulation of the low-temperature HMF distributions in Fe-Ni alloys, we attempted a simulation of the high-temperature HMF distribution. It was hoped that the temperature dependence of the HMF distribution could be largely assigned to one parameter whose variation with temperature accounted for the correct trends in the shape of the Mössbauer spec-

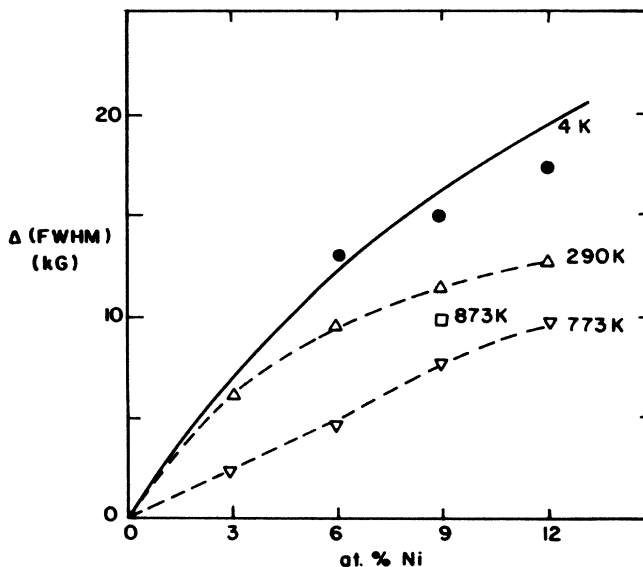


FIG. 7. Change in the mean FWHM of peak numbers 1 and 6 of Fe-Ni with respect to the mean FWHM of pure Fe. Solid curve is from simulated peaks with the parameters of Fig. 3.

tra, even if precise agreement between the simulated and experimental spectra was not achieved. The parameter α_{CP} is not expected to be temperature dependent because it describes electron polarization mechanisms involving tightly bound electrons. We found that the nonlocal hyperfine magnetic field response parameters, $\alpha_{CEP}\{f(r)\}$, are largely temperature independent since the effect of Si solutes on Mössbauer spectra is largely unchanged with temperature. (Although the Si satellites in spectra of Fe-Ni alloys at high temperatures provide information about the mechanism of conduction electron polarization by Fe atoms, it is expected that the analogous mechanism of conduction electron polarization by Ni atoms will also be temperature independent.)

Since the parameters describing the mechanisms of electron polarization are temperature independent, the temperature dependence of the Fe-Ni HMF distribution must be due to a temperature dependence of the magnetic moments or the magnetic moment perturbations. We reference our Fe-Ni Mössbauer spectra to pure Fe spectra at the same temperature, so the reduction in μ_{Fe} cannot be the cause of the different temperature dependences of the ^{57}Fe HMF in Fe and Fe-Ni alloys. Within our simulation, we can account for the temperature dependence of the mean HMF of Fe-Ni alloys by assuming that either μ_{Ni} or $\{g_{Ni}^{Fe}(r)\}$ is reduced more rapidly with temperature than μ_{Fe} . The variance of the HMF distribution, however, requires that it is the reduction in $\{g_{Ni}^{Fe}(r)\}$ parameters which is responsible for the temperature dependence of the ^{57}Fe HMF distribution in Fe-Ni alloys. Our computer calculation of the HMF distribution showed that if μ_{Ni} were to decrease with temperature, the FWHM of the HMF distribution would simultaneously increase. The opposite experimental systematics are observed. Neutron diffuse magnetic scattering experiments at elevated temperatures by Child and Cable²⁵ also indicate that the Ni magnetic moment is temperature independent.

The $\{g_{Ni}^{Fe}(r)\}$ parameters were reduced so as to reproduce the correct mean HMF at higher temperatures by multiplying the set of $\{g_{Ni}^{Fe}(r)\}$ parameters at low temperatures by the factors 0.7, 0.1 + and -0.2 for the temperatures 290 K, 773, and 873 K, respectively (see solid curves in Fig. 4). With these parameters for increasing temperature, the FWHM of the calculated HMF distribution decreases up to 773 K, and then increases again in qualitative agreement with the experimental trend. However, this decrease in FWHM is not in quantitative agreement with the experimental data of Fig. 7; at 290 K the calculated decrease is about one-third as large as the measured decrease, and the simulated width at 773 K is nearly as large as at 290 K. Much of the discrepancy in the simulated width at higher temperatures can be accounted for with a simultaneous reduction in μ_{Ni} . The required reductions of $\{g_{Ni}^{Fe}(r)\}$ with temperature will then be somewhat smaller, and the $\{g_{Ni}^{Fe}(r)\}$ need not change sign at 873 K. Because the $\alpha_{CEP}\{f(r)\}$ parameters are somewhat controversial,^{3,17,29} we have determined that an alternate set of parameters, $\{-11.0, -0.9, -2.5\}$ kG, similarly indicates that the $\{g_{Ni}^{Fe}(r)\}$ parameters, and not μ_{Ni} , are the source of the temperature dependence.

The temperature dependence of the RFF and the SODS

indicate that the mean-squared thermal displacement $\langle\delta^2\rangle$ and the mean-square thermal velocity $\langle v^2\rangle$ of ^{57}Fe atoms in Fe-Ni alloys is greater than in pure Fe at the same temperature. We suggest that the anomalous temperature dependence of the $\{g_{Ni}^{Fe}(r)\}$ parameters results from the large thermal motion of the ^{57}Fe atoms in Fe-Ni alloys. We offer two explanations for this involving the spin-dependent charge transfers between Fe and Ni neighbors, which are the source of the $\{g_{Ni}^{Fe}(r)\}$. Our first explanation is analogous to the Debye-Waller factor for coherent scattering. The Fourier components of the lattice periodic potential U_k , will be reduced as $e^{-k^2\langle\delta^2\rangle/3}$. We expect that the spin-dependent charge transfers between Fe and Ni atoms will also show a similar dependence on thermal displacements. The $\{g_{Ni}^{Fe}(r)\}$ parameters are more temperature dependent than the RFF. For this Debye-Waller analog to account for the temperature dependence of the $g_{Ni}^{Fe}(r)$ parameters, the important k vectors for the spin-dependent charge transfers must be greater than k_γ ($\approx 7 \text{ \AA}^{-1}$), which is reasonable if the charge transfers involve short-range interactions. We also offer a second explanation. The spin-dependent charge transfers are sensitive to the radial separation between the Fe and Ni atoms. Only a small dependence of these charge transfers on $(d/dr)g_{Ni}^{Fe}(r)$ is expected because the differences in thermal expansion between pure Fe and Fe-Ni are only $\sim 10^{-4}$ over the temperature range 4 to 873 K.⁴¹ However, when we thermally average a Taylor approximation for $g_{Ni}^{Fe}(r+\delta)$, the term $(\langle\delta^2\rangle/2)(d^2/dr^2)g_{Ni}^{Fe}(r)$ is nonvanishing. Hence the $g_{Ni}^{Fe}(r)$ will decrease more rapidly than μ_{Fe} if $(d^2/dr^2)g_{Ni}^{Fe}(r)$ is strongly negative. We have not attempted a realistic estimate of this second effect.

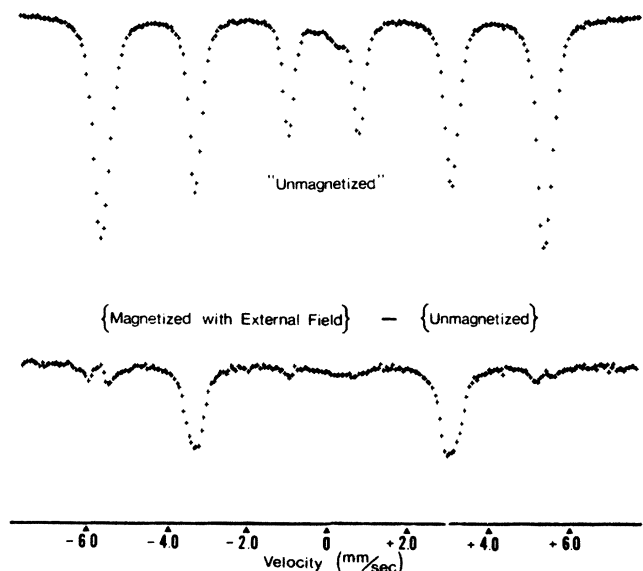


FIG. 8. Top: spectrum of Fe-8.86 at. % Ni taken without an applied magnetic field at 290 K. Bottom: difference between spectra of Fe-8.86 at. % Ni with and without an applied 2.2-kG magnetic field. (Same scales of abscissa and ordinate for top and bottom.)

D. Magnetization direction and HMF distribution

During the course of this work we found that the shape of the HMF distribution from Fe-Ni alloys was slightly sensitive to the direction of magnetization in the specimen. Although this effect was not explored in detail with single crystals of Fe-Ni, it probably results from a pseudodipolar interaction of the type reported by Cranshaw for Fe-Si and Fe-Cr alloys^{29,42} and by Schwartz and Asano⁴³ for Fe-Mo. As shown by Fig. 8, an applied homogeneous saturating magnetic field that forces the specimen magnetization to lie perpendicular to the incident γ rays gives a HMF distribution that is wider than the HMF distribution observed when the domain magnetizations were random with respect to the incident γ -ray direction. (No such effect was seen for specimens of pure Fe.) Without an applied magnetic field the domain magnetizations tend to lie along the easy [100] axis, and 1NN Ni atoms, which are situated at an angle of 53.7° with respect to [100], produce a vanishing pseudodipolar contribution [$3 \cos^2(53.7^\circ) - 1 = 0$]. With an applied magnetic field the 1NN Ni atoms will be situated at random with respect to the magnetic field direction, so the 1NN Ni atoms can produce nonzero pseudodipolar contributions. This results in an increased width of the HMF distribution. It was necessary to impose a standard condition of magnetization on specimens when small changes in Ni concentration ($\sim 0.1\%$) were to be determined.¹⁸ However, none of the results described in the present work were significantly affected by the direction of specimen magnetization.

V. CONCLUSION

A model of linear response of ^{57}Fe HMF's to local magnetic moments is supported by our understanding of the mechanisms of electron polarization at the ^{57}Fe nucleus, and by experimental systematics. The model accurately predicts the shapes of Mössbauer spectra of Fe-Ni alloys at low temperatures. A marked difference was observed

between the temperature dependence of the ^{57}Fe HMF distribution in Fe-Ni alloys and the temperature dependence of the ^{57}Fe HMF in pure Fe. By measuring the effects of 1NN and 2NN Si atoms on the ^{57}Fe HMF, it was shown that the conduction electron polarization mechanisms are largely independent of temperature and Ni concentration. Simulations of the ^{57}Fe HMF distribution in Fe-Ni alloys indicate that the $\{g_{\text{Ni}}^{\text{Fe}}(r)\}$ parameters are the major source of this anomalously strong temperature dependence, although a rapid reduction in $\langle\mu_{\text{Ni}}\rangle$ may be important at higher temperatures. It was also found that the RFF had a stronger temperature dependence in Fe-Ni alloys than in pure Fe, and this accounts for most of the temperature dependence of the mean position of the spectrum. We suggest that the large thermal displacements responsible for the lower RFF of Fe-Ni alloys are also responsible for the temperature dependence of the $\{g_{\text{Ni}}^{\text{Fe}}(r)\}$ parameters. The disturbance of lattice periodicity by thermal displacements should reduce the $\{g_{\text{Ni}}^{\text{Fe}}(r)\}$ as $e^{-k^2(\delta^2)/3}$. Alternatively, the spin-dependent charge transfers responsible for the $\{g_{\text{Ni}}^{\text{Fe}}(r)\}$ parameters may be reduced if $(d^2/dr^2)g_{\text{Ni}}^{\text{Fe}}(r)$ is strongly negative.

We have also observed effects of applied magnetic fields on Mössbauer peaks of Fe-Ni that indicate the presence of a pseudodipole component of the ^{57}Fe HMF perturbations around Ni atoms. Finally, we have pointed out difficulties in parameterizing HMF perturbations in terms of solute occupancies of nearest-neighbor shells when the solutes strongly perturb the magnetic moments of neighboring Fe atoms.

ACKNOWLEDGMENTS

The authors are grateful to T. Lindsey for important discussions and suggestions. This work was supported by the Director, Office of Energy Research, Office of Basic Energy Science, Materials Science Division of the U.S. Department of Energy under Contract No. DE-AC03-76SF00098.

*Present address: Keck Laboratory of Engineering, California Institute of Technology, Pasadena, California 91125.

¹P. J. Schurer, K. W. Maring, F. Van der Woude, and G. A. Sawatzky, *Int. J. Magn.* **4**, 291 (1973); **4**, 297 (1973).

²F. van der Woude and G. A. Sawatzky, *Phys. Rep.* **12**, 335 (1974).

³I. Vincze and L. Cser, *Phys. Status Solidi B* **50**, 709 (1972).

⁴I. Vincze, *Solid State Commun.* **10**, (1972) 341.

⁵I. Vincze and G. Grüner, *Phys. Rev. Lett.* **28**, 178 (1972).

⁶P. C. Riedi, *Phys. Lett.* **16**, 273 (1970).

⁷P. C. Riedi, *J. Phys. F* **3**, 206 (1973).

⁸P. C. Riedi, *J. Phys. F* **8**, L95 (1978).

⁹P. C. Riedi, *J. Phys. F* **8**, L201 (1978).

¹⁰J. I. Budnick, T. J. Burch, S. Skalski, and K. Raj, *Phys. Rev. Lett.* **24**, 511 (1970).

¹¹I. Vincze and I. A. Campbell, *J. Phys. F* **3**, 647 (1973).

¹²I. Vincze, I. A. Campbell, and A. J. Meyer, *Solid State Commun.* **15**, 1495 (1974).

¹³D. A. Shirley and G. A. Westenbarger, *Phys. Rev.* **138**, A170 (1965).

¹⁴M. B. Stearns and S. S. Wilson, *Phys. Rev. Lett.* **13**, 313 (1964).

¹⁵M. B. Stearns, *Phys. Rev. B* **4**, 4069 (1971); **4**, 4081 (1971).

¹⁶M. B. Stearns, *Phys. Rev. B* **9**, 2311 (1974).

¹⁷M. B. Stearns, *Phys. Rev. B* **13**, 1183 (1976).

¹⁸B. Fultz and J. W. Morris, Jr., in *Industrial Applications of the Mössbauer Effect*, edited by G. Long and J. Stevens (Plenum, New York, 1986).

¹⁹R. E. Watson and A. J. Freeman, *Phys. Rev.* **123**, 2027 (1961); in *Hyperfine Interactions*, edited by A. J. Freeman and R. B. Frankel (Academic, New York, 1967), Chap. 2.

²⁰K. J. Duff and T. P. Das, *Phys. Rev. B* **12**, 3870 (1975).

²¹T. Yang, A. Kreshnan, and N. Benczer-Koller, *Phys. Rev. B* **30**, 2438 (1984).

²²G. K. Wertheim, V. Jaccarino, J. H. Wernick, and D. N. E. Buchanan, *Phys. Rev. Lett.* **12**, 24 (1964).

- ²³T. M. Holden, J. B. Comly, and G. G. Low, Proc. Phys. Soc. London **92**, 726 (1967).
- ²⁴G. G. Low, J. Appl. Phys. **39**, 1174 (1968).
- ²⁵H. R. Child and J. W. Cable, Phys. Rev. B **13**, 227 (1976).
- ²⁶M. B. Stearns and L. A. Feldkamp, Phys. Rev. B **13**, 1198 (1976).
- ²⁷These parameters were $\alpha_{CP} + \alpha_{CEP} = -90.5$ kG/ μ_B , $\alpha_{CEP}\{f(r_j)\} = \{-12.1, -2.7, +2.4\}$ kG/ μ_B , $\mu_{Fe} = 2.2\mu_B$, $\mu_{Ni} = 1.4\mu_B$, $\{g_{Ni}^{Fe}(r_j)\} = \{.093, .062, .022, .013, .012, 0, \dots\}$, $\{g_{Ni}^{Ni}(r_j)\} = \{0\}$.
- ²⁸However, in her sum of average contributions to the HMF in the equation following her Eq. (8) in Ref. 16, the neglect of Fe magnetic moments in fifth and sixth nearest-neighbor shells from the ⁵⁷Fe atoms results in a mean HMF perturbation that is underestimated by 20%. She compared this underestimated mean HMF to room temperature measurements of the mean HMF, which are about 35% smaller than those at cryogenic temperatures, leading to a similar discrepancy with a less appropriate analysis.
- ²⁹T. E. Cranshaw, C. E. Johnson, M. S. Ridout, and G. A. Murray, Phys. Lett. **21**, 481 (1966).
- ³⁰M. F. Collins and G. G. Low, Proc. Phys. Soc. London **86**, 535 (1965).
- ³¹I. A. Campbell, Proc. Phys. Soc. London **89**, 71 (1966).
- ³²A. T. Pickles and W. Sucksmith, Proc. R. Soc. London **175**, 331 (1940).
- ³³J. Crangle and G. C. Hallam, Proc. R. Soc. London, Ser. A **272**, 119 (1963).
- ³⁴D. I. Bardos, J. L. Beeby, and A. T. Aldred, Phys. Rev. **177**, 878 (1969).
- ³⁵C. G. Shull and M. K. Wilkinson, Phys. Rev. **97**, 304 (1955).
- ³⁶M. F. Collins, R. V. Jones, and R. D. Lowde, J. Phys. Soc. Jpn. **17**, Suppl. B III, 19 (1962).
- ³⁷M. F. Collins and J. B. Forsyth, Philos. Mag. **8**, 401 (1963).
- ³⁸R. S. Preston, S. S. Hanna, and J. Heberle, Phys. Rev. **128**, 2207 (1962).
- ³⁹H. M. Ledbetter, in *Advances in Cryogenic Engineering* edited by K. D. Timmerhaus, R. P. Reed, and A. F. Clark (Plenum, New York, 1978), Vol. 24, p. 103.
- ⁴⁰R. E. Watson and L. H. Bennett, Phys. Rev. B **18**, 6439 (1978).
- ⁴¹F. Schwartzberg, *Cryogenic Materials Data Handbook, Vol. II* (U.S. Dept. of Commerce, Boulder, Colorado, 1970), p. 181.
- ⁴²T. E. Cranshaw, J. Phys. F **2**, 615 (1972).
- ⁴³L. H. Schwartz and A. Asano, J. Phys. (Paris), Colloq. **35**, Suppl. C-6, 453 (1974).